nature cell biology

Caspase-11 regulates cell migration by promoting Aip1–Cofilin-mediated actin depolymerization

Juying Li[1], William M. Brieher[2], M. Lucila Scimone[3], Shin Jung Kang[1,5], Hong Zhu[1], Helen Yin[4], Ulrich H. von Andrian[3], Timothy Mitchison[2] and Junying Yuan[1,6]

Coordinated regulation of cell migration, cytokine maturation and apoptosis is critical in inflammatory responses. Caspases, a family of cysteine proteases, are known to regulate cytokine maturation and apoptosis. Here, we show that caspase-11, a mammalian pro-inflammatory caspase, regulates cell migration during inflammation. Caspase-11-deficient lymphocytes exhibit a cell-autonomous migration defect *in vitro* and *in vivo*. We demonstrate that caspase-11 interacts physically and functionally with actin interacting protein 1 (Aip1), an activator of cofilin-mediated actin depolymerization. The caspase-recruitment domain (CARD) of caspase-11 interacts with the carboxy-terminal WD40 propeller domain of Aip1 to promote cofilin-mediated actin depolymerization. Cells with Aip1 or caspase-11 deficiency exhibit defects in actin dynamics. Using *in vitro* actin depolymerization assays, we found that caspase-11 and Aip1 work cooperatively to promote cofilin-mediated actin depolymerization. These data demonstrate a novel cell autonomous caspase-mediated mechanism that regulates actin dynamics and mammalian cell migration distinct from the receptor mediated Rho–Rac–Cdc42 pathway.

Caspase-11 is a critical activator of caspase-1 in lipopolysaccharide (LPS)-induced IL-1β maturation[1,2]. The expression of caspase-11 is barely detectable in most tissues of healthy mice, but is highly inducible on LPS injection and stress[2]. *Caspase-11*$^{-/-}$ mice are severely defective in IL-1β maturation and secretion after LPS stimulation, and are resistant to LPS-induced septic shock[3]. Caspase-11 is also involved in directly activating caspase-3 and apoptosis under certain pathological conditions[4,5]. Therefore, caspase-11 has an important dual role in regulating both inflammatory response and apoptosis.

In motile cells, actin filaments organize into a branched network at the leading edge, and the filaments undergo rapid and coordinated assembly and/or disassembly to drive the edge forward[6]. The dynamics and organization of the actin network are regulated by many actin-binding proteins. The activity of cofilin, a major actin-depolymerization factor, can be positively modulated by actin interacting protein 1 (Aip1)[7–9]. Aip1 has been shown to regulate the motility of *Dictyostelium* amoeboid cells[10], but a functional role for Aip1 in mammalian cell migration has not been established.

An intriguing genetic study in *Drosophila* identified a possible role for caspases in mediating ovary-border cell migration[11]. Overexpression of *Drosophila* inhibitor of apoptosis (DIAP1, a direct inhibitor of caspases in *Drosophila*), and mutations in Dark (an activator of the upstream caspase Dronc) rescued the migration defect caused by a dominant-negative Rac mutation. Furthermore, a loss-of-function mutation of DIAP1, in this system, caused migration defects, but not apoptosis. A similar role for caspases in regulating mammalian cell migration is unknown.

Here, we report a novel function of caspase-11 in regulating cell migration. We show that *caspase-11*$^{-/-}$ cells exhibit a cell-autonomous migration defect. We describe an unexpected connection between caspase-11, a caspase directly involved in cellular inflammatory response, and actin dynamics. Our studies indicate that caspase-11 may be a central regulator of multiple events, including cell migration, cytokine maturation and apoptosis, during inflammatory responses.

RESULTS

Caspase-11-deficient leukocytes are defective in migration *in vitro* and *in vivo*

While we were characterizing *caspase-11*$^{-/-}$ mice, we noted a cell-autonomous defect in the migration of *caspase-11*$^{-/-}$ cells. In a transwell migration assay, *caspase-11*$^{-/-}$ splenocytes showed a reduced rate of basal migration and chemokine-induced migration compared with wild-type cells (Fig. 1a), suggesting that caspase-11 may be involved in regulating basal cell motility when it is induced *in vivo* under inflammatory conditions (for example, in response to LPS). To confirm this possibility, the basal random migratory behaviour of wild-type and *caspase-11*$^{-/-}$ peritoneal macrophages was compared using time-lapse microscopy

[1]Department of Cell Biology, Harvard Medical School, 240 Longwood Ave, Boston, MA 02115, USA. [2]Department of Systems Biology, Harvard Medical School, 240 Longwood Ave, Boston, MA 02115, USA. [3]The CBR Institute for Biomedical Research, Harvard Medical School, 240 Longwood Ave, Boston, MA 02115, USA. [4]Department of Physiology, UT Southwestern Medical Center at Dallas, 5323 Harry Hines Blvd, Dallas, TX 75390, USA. [5]Current address: Department of Molecular Biology, Sejong University, Seoul 143-747, Korea. [6]Correspondence should be addressed to J.Y. (e-mail: jyuan@hms.harvard.edu)

Received 21 November 2006; accepted 17 January 2007; published online 11 February 2007; DOI: 10.1038/ncb1541

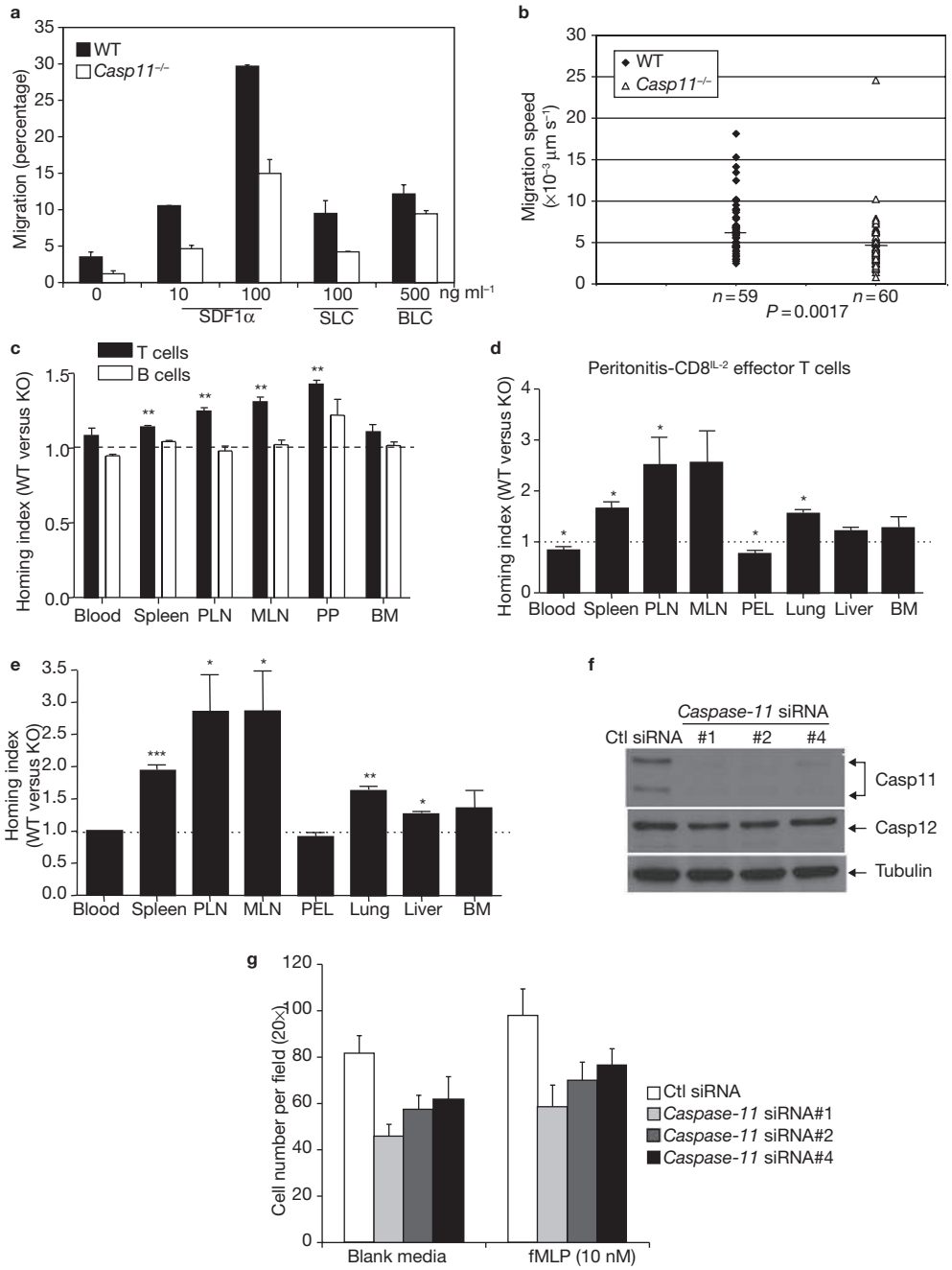

Figure 1 *Caspase-11*$^{-/-}$ splenocytes and peritoneal macrophages are defective in cell migration *in vitro* and *in vivo*. (**a**) Migration of wild-type (WT) and *caspase-11*$^{-/-}$ (*casp11*$^{-/-}$) splenocytes towards the indicated chemokines of specified concentrations was determined by percentage of input cells that had migrated to the bottom chambers after 2 h. This is a representative of two independent experiments. The error bars represent s.d. of triplicates. (**b**) Quantification of wild-type and *caspase-11*$^{-/-}$ peritoneal macrophage migration velocity. Migration velocity was calculated as the total distance the cell nucleus moved on the path divided by the total time over 50 frames. The average value of each group is indicated by a dash. The *P* value was calculated using an unpaired Student's *t*-test. This is a representative of two independent experiments. n, cell number. (**c**) Homing behaviours of naïve wild-type and *caspase-11*$^{-/-}$ splenocytes to the secondary lymphoid organs (for details see Methods). The homing index in each organ was compared to one using a paired Student's *t*-test. The double asterisks indicate $P < 0.01$ and the single asterisk indicates $P < 0.05$. BM, bone arrow; KO, knockout. The error bars represent the s.e.m. of the homing index of three recipient mice. (**d**) Homing index of CD8^{+} effector T cells in blood, secondary lymphoid organs, peritoneal exude leukocytes (PELs), lung, liver and bone marrow in a peritonitis model. Six recipient mice were used. (**e**) To account for the difference between wild-type and *caspase-11*$^{-/-}$ cells in the circulation, the homing index in different organs was normalized to that in blood. The error bars represent the s.e.m. of the homing index of six recipient mice. Three asterisks indicate $P < 0.0001$, the double asterisk indicates $P < 0.01$ and the single asterisk indicates $P < 0.05$. (**f**) Knockdown of endogenous *caspase-11* in J774 cells using Dharmacon synthetic siRNA oligos. Ctl siRNA, non-targeting control siRNA oligos. #1, #2 and #4 are three different siRNAs targeting *caspase-11*. (**g**) *Caspase-11*-knockdown J774 cells are defective in migration towards blank media and chemoattractant fMLP in the transwell migration assay. This is a representative of two independent experiments. The error bars represent the s.d. of nine random fields from replicates ($P < 0.01$).

(see Supplementary Information, Movies 1 and 2). Calculating the migration velocity by tracing individual cell nucleus movement showed that *caspase-11*$^{-/-}$ macrophages had significantly lower migration velocity (average value: 4.84×10^{-3} μm s^{-1}) compared with wild-type cells (average value: 6.70×10^{-3} μm s^{-1}; Fig. 1b). *Caspase-11*$^{-/-}$ neutrophils showed a similar migration defect (see Supplementary Information, Fig. S1a, b).

To determine whether caspase-11 regulates cell migration in a cell-autonomous fashion *in vivo*, the homing behaviour of naïve wild-type and *caspase-11*$^{-/-}$ lymphocytes entering the secondary lymphoid organs of an unstimulated wild-type host was compared. The expression of caspase-11 was largely absent in flash-frozen tissues isolated from unstimulated mice[2], however, the *in vitro* manipulation induced caspase-11 expression in naïve splenocyptes (see Supplementary Information, Fig. S1c), albeit at a lower level than that of LPS stimulation[2,5]. Splenocytes isolated from unstimulated wild-type and *caspase-11*$^{-/-}$ mice were differentially fluorescently labelled and coinjected intravenously into unstimulated wild-type recipient mice. Single-cell suspensions of blood, bone marrow and multiple secondary lymphoid organs of the recipient mice collected 1 h after injection were analysed by flow cytometry and the homing of wild-type and *caspase-11*$^{-/-}$ lymphocytes were expressed as a homing index[12] (Fig. 1c). Naïve *caspase-11*$^{-/-}$ T cells were defective in homing to multiple organs, including spleen, peripheral lymph nodes (PLNs), mesenteric lymph nodes (MLNs) and Peyer's patches (PPs).

As the main known function of caspase-11 is to regulate inflammation in response to infection of bacterial products[2,3], we compared the homing behaviour of wild-type and *caspase-11*$^{-/-}$ effector T cells in a peritonitis model[13]. Consistent with a migration defect, *caspase-11*$^{-/-}$ cells were more numerous in the blood than wild-type cells, but less than wild-tpe cells in spleen, PLNs and lung (Fig. 1d). Taking into account the circulation efficiency, the homing efficiency was calculated by dividing the homing index in different organs by homing index in the blood of the same mouse (Fig. 1e). The homing efficiency of wild-type CD8^{+} effector T cells was significantly higher than that of *caspase-11*$^{-/-}$ cells in spleen, PLNs, MLNs, lung and liver.

To confirm the effect of caspase-11 on migration, we generated *caspase-11* knockdown J774 cells (a macrophage-like cell line) using short interfering RNA (siRNAs) oligonucleotides. In a transwell migration assay, *caspase-11* knockdown cells (Fig. 1f) migrated significantly slower toward blank media and the chemoattractant fMLP than control cells (Fig. 1g). From these results, we conclude that caspase-11 deficiency leads to a specific migration defect.

Caspase-11 interacts with Aip1

To understand the molecular mechanism by which caspase-11 regulates cell migration, we used an affinity-purification approach to identify caspase-11-binding proteins. Stable J774 cell lines were generated that expressed a Flag-tagged enzymatic-activity site (C254G) mutant form of caspase-11 (J774-C11^{C254G}) or control vector (J774-pBabe). The *caspase-11* mRNA is translated into two products with relative molecular masses (M_r) 43,000 and 38,000 due to the differential usage of two alternative translation initiation sites: the 43K form, but not the 38K form, of caspase-11 contains the intact CARD domain at the amino terminus[5]. The use of caspase-11 active-site mutant eliminated the possible cell-death effect of exogenous caspase-11 expression. As J774 cells constitutively express relatively high levels of caspase-11, the expression of Flag-tagged exogenous caspase-11 only increased the total amount of caspase-11 by 1.3 fold, but could be clearly detected after immunoprecipitation (Fig. 2a). Total lysates of LPS treated J774-C11^{C254G} and J774-pBabe cells were affinity purified using an anti-Flag (M2) agarose column and the proteins eluted by the Flag peptide were analysed by SDS–PAGE. A protein species of 66K, identified in affinity purified proteins from J774-C11^{C254G} but not control cells (Fig. 2b), was shown to be mouse Aip1 by mass spectrometry analysis.

To confirm the interaction between Aip1 and caspase-11, Flag-tagged caspase-11 and HA-tagged Aip1 expression constructs were cotransfected into 293T cells. The cell lysates were immunoprecipitated with either anti-Flag (Fig. 2c) or anti-HA agarose beads (Fig. 2d). The immunopurified protein complexes were analysed by western blotting using anti-HA (Fig. 2c) or anti-caspase-11 antibodies (Fig. 2d). The interaction between transfected Aip1 and caspase-11 was detected in both immunoprecipitation experiments. An unrelated protein, Tip48, expressed at similar levels as Aip1, did not interact with caspase-11 (Fig. 2d). A rat monoclonal antibody against mouse Aip1 was generated, which specifically recognizes both endogenous and transfected mouse Aip1 (see Supplementary Information, Fig. S1d). This antibody was used to probe a western blot of the protein eluate from the original affinity purification experiment (Fig. 2b) and confirmed that the 66K protein species eluted from Flag-tagged caspase-11 immunocomplex was mouse Aip1.

In J774 cells, the expression level of caspase-11, but not that of Aip1, was upregulated after LPS stimulation (Fig. 2e and see Supplementary Information, Fig. S1e). The interaction of endogenous Aip1 with caspase-11 in control and LPS-stimulated J774 cells was then examined by immunoprecipitation (Fig. 2e). The amounts of endogenous caspase-11 immunoprecipitated, and the associated Aip1, were both increased after LPS stimulation, consistent with a possible significance for this interaction in inflammation. The interaction between caspase-11 and Aip1 was further confirmed by immunoprecipitation in wild-type splenocyte lysates using *caspase-11*$^{-/-}$ splenocyte lysates as a negative control (see Supplementary Information, Fig. S1f).

The Aip1 protein contains 14 WD40 repeats, which make up two propellers (the N-terminal propeller and the C-terminal propeller, structural motifs that mediate protein–protein interactions). Each WD40 repeat is made up of four anti-parallel β-strands. Interestingly, the N-terminal first β-strand (around 10 amino acids) of Aip1 completes the last WD40 repeat formation with the other three β-strands at the end of C-terminal propeller[14]. To characterize the mechanism by which caspase-11 and Aip1 interact, a series of expression constructs were generated for the wild-type full length and truncated mutants of Aip1 and caspase-11 (Fig. 2f). The full-length caspase-11 coprecipitated with the intact C-terminal propeller (with the N-terminal first β-strand) or full-length Aip1, but not the C-terminal propeller without the N-terminal first β-strand or the N-terminal propeller (Fig. 2g). The domains of caspase-11 can be divided into the N-terminal CARD and the p30 domain, the latter which contains the cysteine protease activity (Fig. 2f). Coimmunoprecipitation results revealed that the full-length or the CARD domain of caspase-11 interacts with Aip1, but not the p30 domain (Fig. 2h). Taken together, these results show that the C-terminal WD40 propeller of Aip1 and the CARD domain of caspase-11 mediate the interaction between these two proteins.

Aip1-knockdown cells are defective in migration

To study the effect of Aip1 deficiency on mammalian cell migration, we generated four J774 cell lines stably expressing control vector

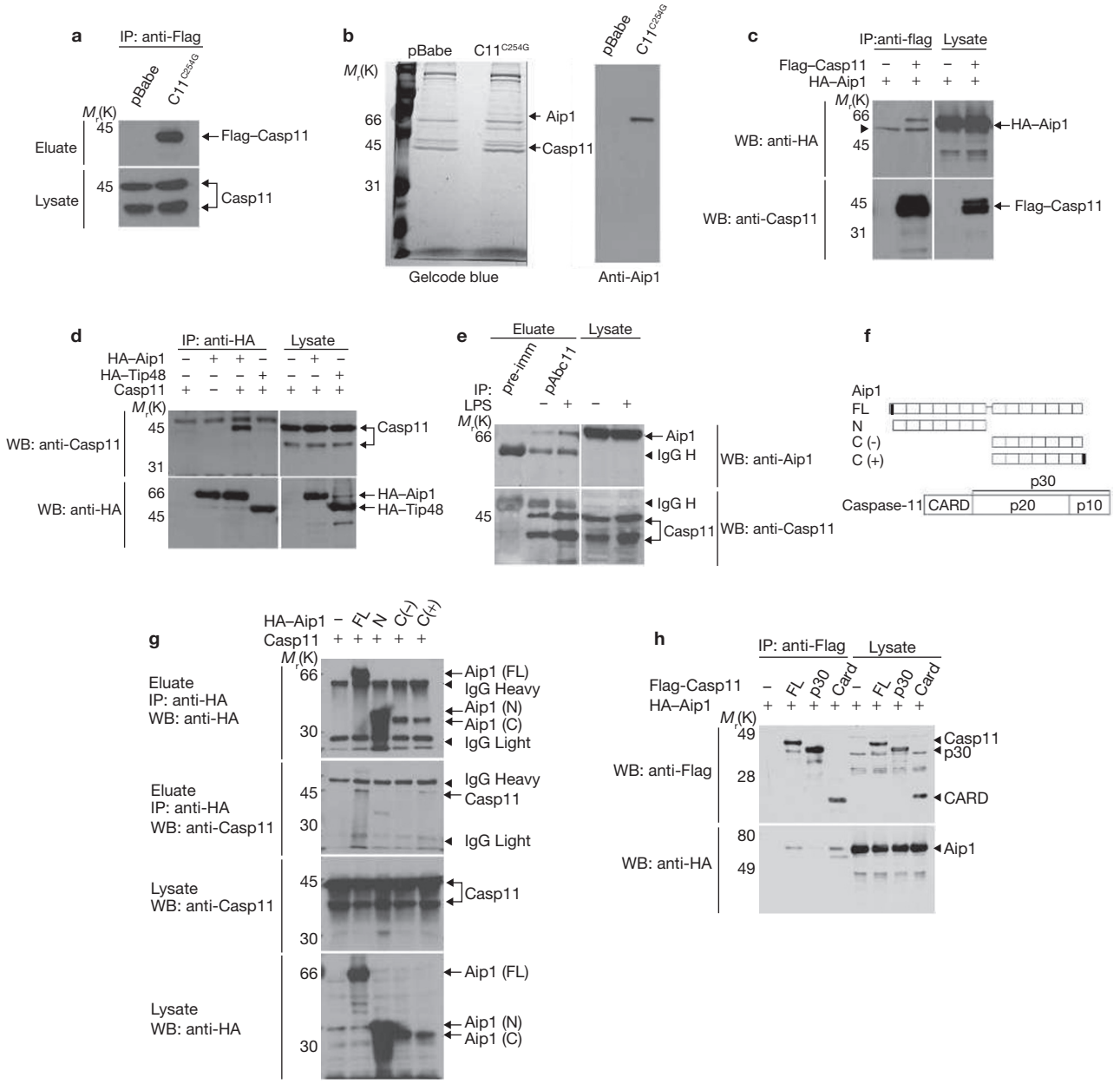

Figure 2 Identification of Aip1 as a caspase-11-interacting protein by affinity purification. (**a**) The expression of caspase-11 in J774 C11^{C254G} cells. Cell lysates of J774 cells stably expressing an N-terminal Flag-tagged caspase-11 active site mutant (C11^{C254G}) or vector alone (pBabe) were immunoprecipitated with anti-Flag M2 agarose beads. The western blots of immunocomplexes and lysate input were probed with anti-caspase-11 antibody. (**b**) Affinity purification of caspase-11 interacting proteins. Proteins in the total lysates of C11^{C254G} and control cells that bound to an anti-Flag M2 agarose column were separated by 12% SDS–PAGE and stained by Gelcode blue. (**c**, **d**) The cell lysates of 293T cells expressing the indicated expression constructs were immunoprecipitated with anti-Flag M2 beads (**c**) or anti-HA beads (**d**). Western blots of the immunocomplexes and lysate input were probed with anti-HA or anti-caspase-11 antibody. The arrowhead points to IgG heavy chain in **c**. (**e**) Cell lysates of control and 10 h LPS-treated J774 cells were immunoprecipitated with rabbit polyclonal anti-caspase-11 antibody (pAb c11) or pre-immune serum (Pre-imm) as a control. The western blots of immunocomplexes and lysate input were probed with anti-Aip1 or anti-caspase-11 monoclonal antibodies. (**f**) A schematic representation of mouse Aip1 constructs and caspase-11. FL, full-length Aip1; N, the N-terminal propeller domain of Aip1; C (–), the C-terminal propeller domain of Aip1 (without the N-terminal first β-strand); C (+), the C-terminal propeller domain of Aip1 (with the N-terminal first β-strand, indicated by the dark rectangle). (**g**) The C-terminal propeller of Aip1 interacts with caspase-11. The cell lysates of 293T cells expressing equal amounts of the indicated expression constructs were immunoprecipitated with anti-HA agarose beads. The western blots of immunocomplexes and lysate input were probed with anti-HA or anti-caspase-11 antibodies. (**h**) The CARD domain of caspase-11 interacts with Aip1. The cell lysates of 293T cells expressing equal amounts of the indicated expression constructs were immunoprecipitated with anti-Flag M2 beads. The western blots of immunocomplexes and lysate input were probed with anti-Flag or anti-HA antibodies.

(psrp), *Aip1* RNAi (*Aip1* RNAi1 & RNAi2) or a point mutant of *Aip1* RNAi1 (*Aip1*^{mut} RNAi1) by retroviral infection. The expression of *Aip1* RNAi1 and *Aip1* RNAi2 caused an 86% and 66% reduction in the endogenous Aip1 levels, respectively, whereas *Aip1*^{mut} RNAi1 had no effect (Fig. 3a). The reduction of Aip1 expression did not lead to an evident change in cell morphology or in the growth rate of J774 *Aip1*

RNAi cells compared with that of control (data not shown). In the transwell migration assay[15], both lines of J774 *Aip1* RNAi cells exhibited significantly slower migration rate towards blank media and also towards two macrophage chemoattractants, MCP1 and fMLP, than that of vector (psrp) or mutant RNAi (*Aip1*^{mut} RNAi1) control cells (Fig. 3b). Expression of an RNAi non-targetable *Aip1* cDNA in *Aip1* RNAi1 cells partially rescued the migration defect in *Aip1* RNAi1 cells (see Supplementary Information, Fig. S2a, b).

To characterize the possible mechanism responsible for the migration defect in *Aip1* RNAi cells, the total amounts of F-actin were compared using a phalloidin–FITC assay[16]. J774 *Aip1* RNAi1, but not *Aip1* RNAi2, cells had ~30% higher amounts of total F-actin than control J774 cells (see Supplementary Information, Fig. S2c). In the two transient *Aip1*-knockdown cells, which also showed the migration defect, total F-actin content was not affected (see Supplementary Information, Fig. S2d–f). Therefore, an increase in the total cellular F-actin amount (as in *Aip1* RNAi1 cells) is not necessary to cause the migration defect.

To further explore the mechanism responsible for the migration defect in both *Aip1* RNAi cells, we examined the localized actin dynamics associated with fMLP-induced membrane ruffling[17], as the reduction of Aip1 expression has been shown to reduce lamella formation in *Drosophila* S2 cells[18] and actin-filament disassembly is important for protrusion of the lamellipodium during cell migration[19]. In this assay, the addition of fMLP to cells after 1 h of serum starvation induced F-actin-rich membrane ruffle formation, which peaked at 1 min (Fig. 3c, d) and subsided to the basal levels after 10 min in control cells. In comparison, F-actin-positive membrane ruffle formation in both *Aip1* RNAi cell lines (*Aip1* RNAi1 and *Aip1* RNAi2) was much weaker, even at 1 min, with only localized small patches of ruffling observed when ruffling formation in control cells (psrp and *Aip1*^{mut} RNAi1) was a peak (1 min) and subsided to basal levels after 2 min (Fig. 3c, d). The same defect was observed in transient *Aip1*-knockdown cells (see Supplementary Information, Fig. S2g). This result suggests that Aip1 may play an important role in organizing the dynamics of localized F-actin formation. As cofilin regulates cell polarity during cell migration[20], and cofilin has been shown to undergo rapid dephosphorylation in fMLP-stimulated neutrophils within 1 min and translocate to ruffled membranes[21], a localized change in cofilin-mediated actin dynamics caused by a reduction in Aip1 expression may be sufficient to impair cell migration.

As caspase-11 and Aip1 interact with each other and both caspase-11- and Aip1-deficient cells exhibit a migration defect, we wondered whether elevated expression of caspase-11 may help to correct the migration defect caused by reduced Aip1 expression. The two J774 stable cell lines described in Fig. 2a (J774-pBabe and J774-C11^{C254G}) were infected with *Aip1* RNAi (*Aip1* RNAi1) retrovirus. As both pBabe vector and *Aip1* RNAi vector (psrp) carry the same puromycin selection marker, acute infection was performed without selection. The infection of *Aip1* RNAi retrovirus reduced the expression of endogenous Aip1 levels by ~55% (Fig. 3e). Interestingly, although *Aip1* RNAi cells (pBabe + *Aip1* RNAi) still migrated significantly slower than parental cells (pBabe and C11^{C254G}), increased expression of the caspase-11 active-site mutant in *Aip1* RNAi cells (C11^{C254G} + *Aip1* RNAi) rescued the migration defect to control levels (Fig. 3f), providing evidence for a functional interaction between caspase-11 and Aip1 in regulating cell migration.

Caspase-11 promotes cofilin- and Aip1-dependent actin depolymerization

To examine a possible role for caspase-11 in regulating actin dynamics, we first compared the fMLP-induced ruffling formation in wild-type versus *caspase-11*$^{-/-}$ peritoneal macrophages using the same assay as in Fig. 3c. At each time point, there were more *caspase-11*$^{-/-}$ cells with no ruffling at all than in wild-type cells (Fig. 4a). In the *caspase-11*$^{-/-}$ cells which did form ruffles, the extent of ruffling formation was much weaker than in wild-type cells (as quantified by ruffling index; Fig. 4b).

The total amount of F-actin amount was also compared in wild-type and *caspase-11*$^{-/-}$ splenocytes isolated from littermates. Freshly isolated wild-type and *caspase-11*$^{-/-}$ splenocytes showed a similar cellular composition (percentage of T cells and B cells) and cell size (see Supplementary Information, Fig. S3a, b). The basal total amount of F-actin per cell was not significantly different (see Supplementary Information, Fig. S3c). Wild-type and *caspase-11*$^{-/-}$ splenocytes also have similar expression levels of SDF-1α receptor CXCR4 (data not shown) and the dynamics of actin polymerization induced by SDF-1α[22] were analysed. In response to SDF-1α stimulation, the total amounts of F-actin peaked within 1 min and reduced to steady-state levels after 2 min in both wild-type and *caspase-11*$^{-/-}$ splenocytes (Fig. 4c and see Supplementary Inforamtion, Fig. S3c). Interestingly, actin polymerization occurred faster in *caspase-11*$^{-/-}$ splenocytes than in wild-type cells, as indicated by the steeper uphill slope of the polymerization curve for *caspase-11*$^{-/-}$ cells than for wild-type cells. This result suggests that caspase-11 may regulate chemokine-stimulated actin polymerization and/or depolymerization.

To directly examine whether caspase-11 can influence the rate of actin depolymerization, we performed an *in vitro* actin-filament depolymerizaton assay[23]. Texas-red labelled actin monomers were mixed with unlabelled actin monomers at a 1:1 ratio to form actin filaments *in vitro*. The presence of cofilin (2 μM) promoted actin-filament depolymerization within 5 min of incubation (Fig. 5A a, b). The presence of Aip1 (100 nM) in this system augmented the destabilization effect of cofilin (see Supplementary Information, Fig. S3d). To detect a possible effect of recombinant caspase-11 in promoting Aip1- and cofilin-dependent depolymerization, a suboptimal concentration of Aip1 (50 nM) was used that did not affect cofilin-mediated actin depolymerization significantly (Fig. 5A c, d and see Supplementary Information, Fig. S3d). Interestingly, the addition of recombinant caspase-11 (1 μM) together with Aip1 dramatically increased cofilin-mediated actin depolymerization (Fig. 5A g, h). Recombinant caspase-11 alone had no significant effect on cofilin-mediated actin depolymerization (Fig. 5A e, f).

An actin-filament pelleting assay[24] was used to confirm the ability of caspase-11 to promote actin depolymerization. Cofilin alone started to show significant actin depolymerization activity in this assay system at a concentration of 8 μM (see Supplementary Information, Fig. S3e). Aip1 (50 nM) together with cofilin did not increase the presence of actin in the supernatant fraction significantly (Fig. 5B, lanes 7, 8) compared with cofilin alone (Fig. 5B, lanes 3, 4). However, the addition of recombinant caspase-11 (1 μM), together with cofilin and Aip1, dramatically increased the fraction of actin in the supernatant (Fig. 5B, lanes 9, 10). The effect of caspase-11 on actin depolymerization was not altered in the presence of a pan-caspase inhibitor, zVAD.fmk, indicating that caspase activity may not be required for caspase-11 to promote actin depolymerization in this assay (Fig. 5B, lanes 11, 12). Recombinant caspase-11 by itself did not promote actin depolymerization (Fig. 5B,

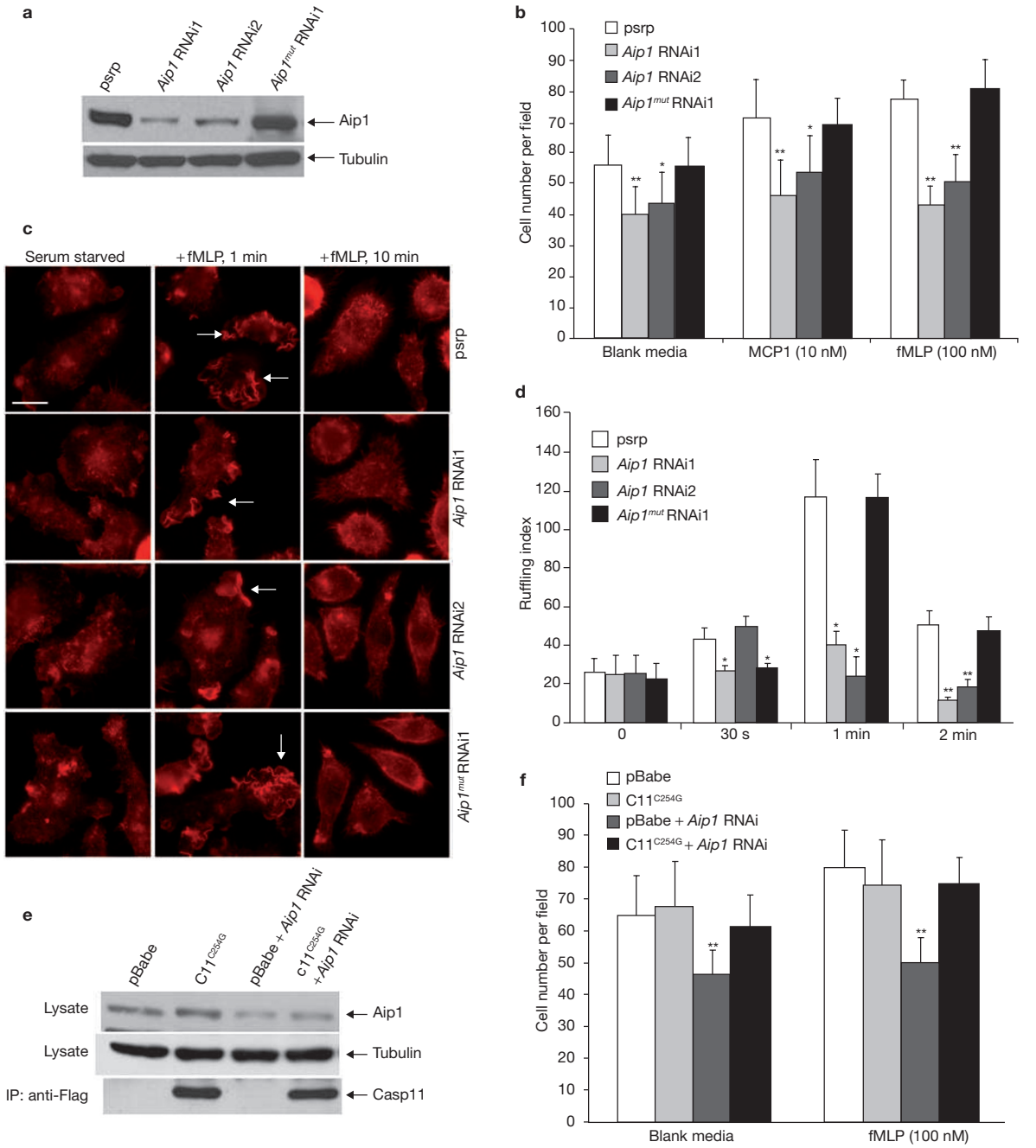

Figure 3 *Aip1* RNAi cells are defective in cell migration *in vitro*. (**a**) A western blot analysis of Aip1 expression in J774 cells expressing the indicated *Aip1* RNAi. (**b**) Migration of J774 control and *Aip1* RNAi cells towards indicated chemoattractants were determined by the number of cells that migrated to the bottom surface of the transwell insert after 2 h. Cell numbers were counted in nine random fields under a 20× objective. Statistics were calculated using an unpaired Student's *t*-test. The double asterisk indicates $P < 0.01$ and the single asterisk indicates $P < 0.05$. The error bars represent the s.d. of nine fields from replicates. The result is a representative of three independent experiments. (**c**) Membrane ruffling formation in fMLP-stimulated J774 control and *Aip1* RNAi cells. F-actin rich membrane ruffles were stained with rhodamine–phalloidin as indicated by arrows. The scale bar represents 18 μm. (**d**) Quantification of fMLP-induced membrane ruffles in J774 control and *Aip1* RNAi cells at the indicated times by ruffling index. The error bars represent the s.d. of the ruffling index of four random fields. This result is a representative of two independent experiments. (**e**) Western blot analysis of Aip1 and caspase-11 expression in parental cells (pBabe, $C11^{C254G}$) and *Aip1* RNAi cells (pBabe + *Aip1* RNAi, $C11^{C254G}$ + *Aip1* RNAi). The pBabe plasmid contains an N-terminal Flag-tag. (**f**) Transwell migration of parental cells (pBabe, $C11^{C254G}$) and *Aip1* RNAi cells (pBabe + *Aip1* RNAi, $C11^{C254G}$ + *Aip1* RNAi) was measured as above. The error bars represent the s.d. of nine fields from replicates. The result is a representative of two independent experiments.

lanes 13, 14), nor did caspase-11 alter the cofilin-dependent actin depolymerization in the absence of Aip1 (Fig. 5B, lanes 5, 6). Recombinant CARD domain or p30 domain of caspase-11 did not affect Aip1- and cofilin- dependent actin depolymerization (data not shown). These results suggest that caspase-11 and Aip1 work cooperatively to promote cofilin-mediated actin depolymerization. Caspase-11 by itself is

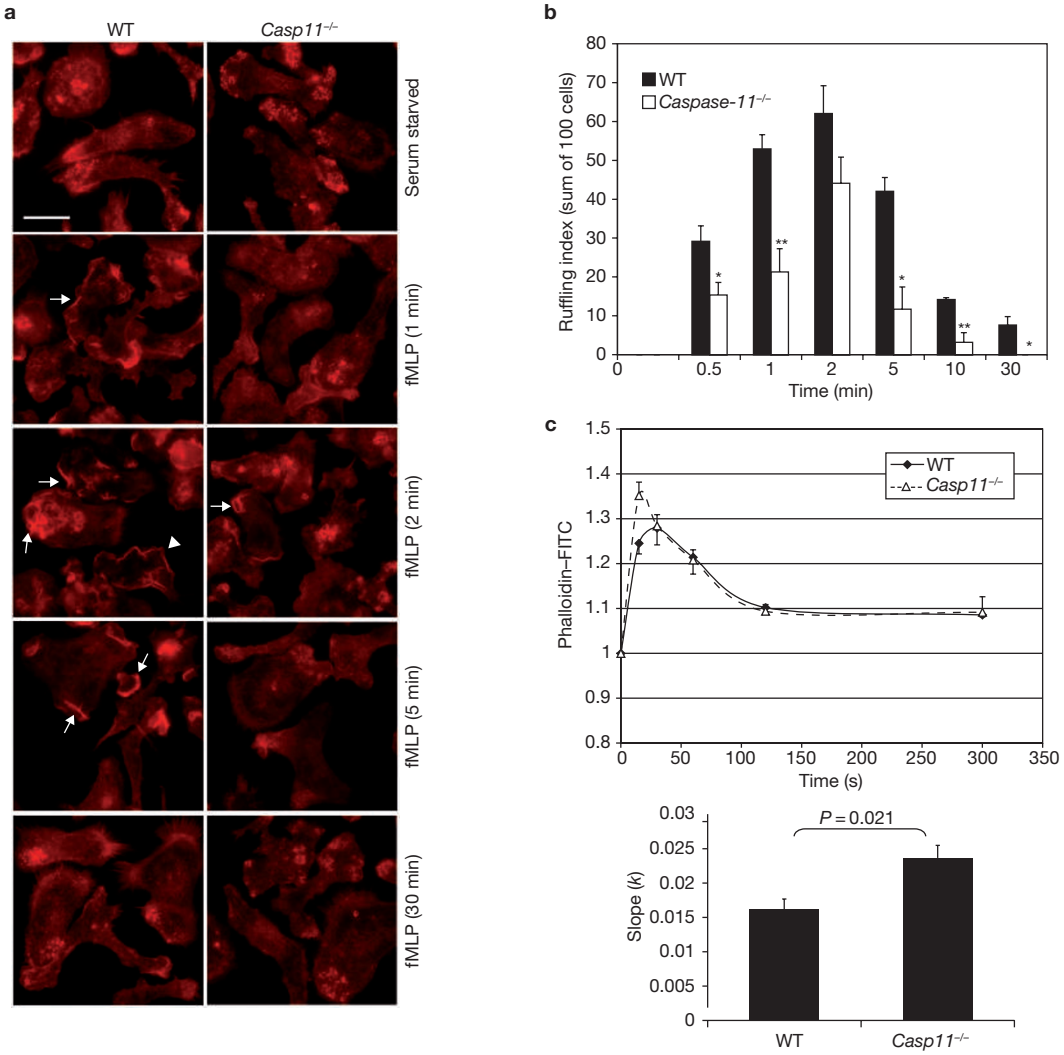

Figure 4 Caspase-11 regulates actin dynamics *in vivo*. (**a**) Wild-type and *caspase-11*$^{-/-}$ peritoneal macrophages were serum starved for 1 h and then stimulated with 100 nM fMLP for the indicated time, as in Fig. 3c. The arrows point to cells with a ruffling score of one. The arrowheads point to cells with a ruffling score of two. The scale bar represents 18 μm. (**b**) The ruffling index of wild-type and *caspase-11*$^{-/-}$ cells was quantified as in Fig. 3d. (**c**) Dynamics of F-actin formation in the splenocytes from littermates of wild-type and *caspase-11*$^{-/-}$ mice in response to SDF-1α. Splenocytes were fixed at the indicated times after the addition of SDF-1α and labelled with FITC–phalloidin. The average amount of FITC–phalloidin incorporated per cell was quantified by FACS and normalized to the value at 0 s. WT, *caspase-11*$^{+/+}$. The figure shown is mean ± s.e.m. of the phalloidin–FITC reading from four independent experiments. The uphill (0–15 s) slope (*k*) of the curve was calculated for every curve in each experiment (total $n = 4$ mice of each genotype). The error bars represent s.e.m. of *k* from four independent experiments.

a soluble protein (Fig. 5B, lanes 15, 16). Interestingly, most of the full-length caspase-11 shifted to the pellet fraction in the presence of actin filament (Fig. 5B, lanes 13, 14). In the presence of cofilin and Aip1, however, a portion of full-length caspase-11 shifted from the pellet fraction into the supernatant fraction (Fig. 5B, lanes 9, 10). These results suggest the intriguing possibility that caspase-11 may be able to bind to the actin filament directly. At the optimal dose (100 nM), Aip1 by itself significantly promoted cofilin-dependent actin depolymerization (see Supplementary Information, Fig. S3f). The ability of caspase-11 to cooperate with Aip1 when Aip1 is at sub-optimal dose (50 nM), even in the presence of zVAD.fmk (Fig. 5B, lanes 11, 12), may explain why the expression of enzymatic inactive caspase-11 could rescue the migration defect in *Aip1* RNAi cells (Fig. 3f).

Cofilin levels are upregulated in *caspase-11*$^{-/-}$ mouse spleen and *Aip1*-knockdown cells

Although the lack of developmental defects in *caspase-11*$^{-/-}$ mice could be explained by its extremely low level of expression under normal conditions[2], we wanted to determine whether the expression levels of cofilin and Aip1 were altered in *caspase-11*$^{-/-}$ mice. Although the expression levels of Aip1 were not altered in the *caspase-11*$^{-/-}$ spleen, the expression level of cofilin was significantly increased (Fig. 6a). This result suggests that the lack of caspase-11 may lead to a compensatory expression of cofilin, providing *in vivo* evidence to support the role of caspase-11 in promoting cofilin-mediated actin depolymerization. To examine whether reduced expression of Aip1 would lead to similar compensatory changes of gene expression, the levels of caspase-11,

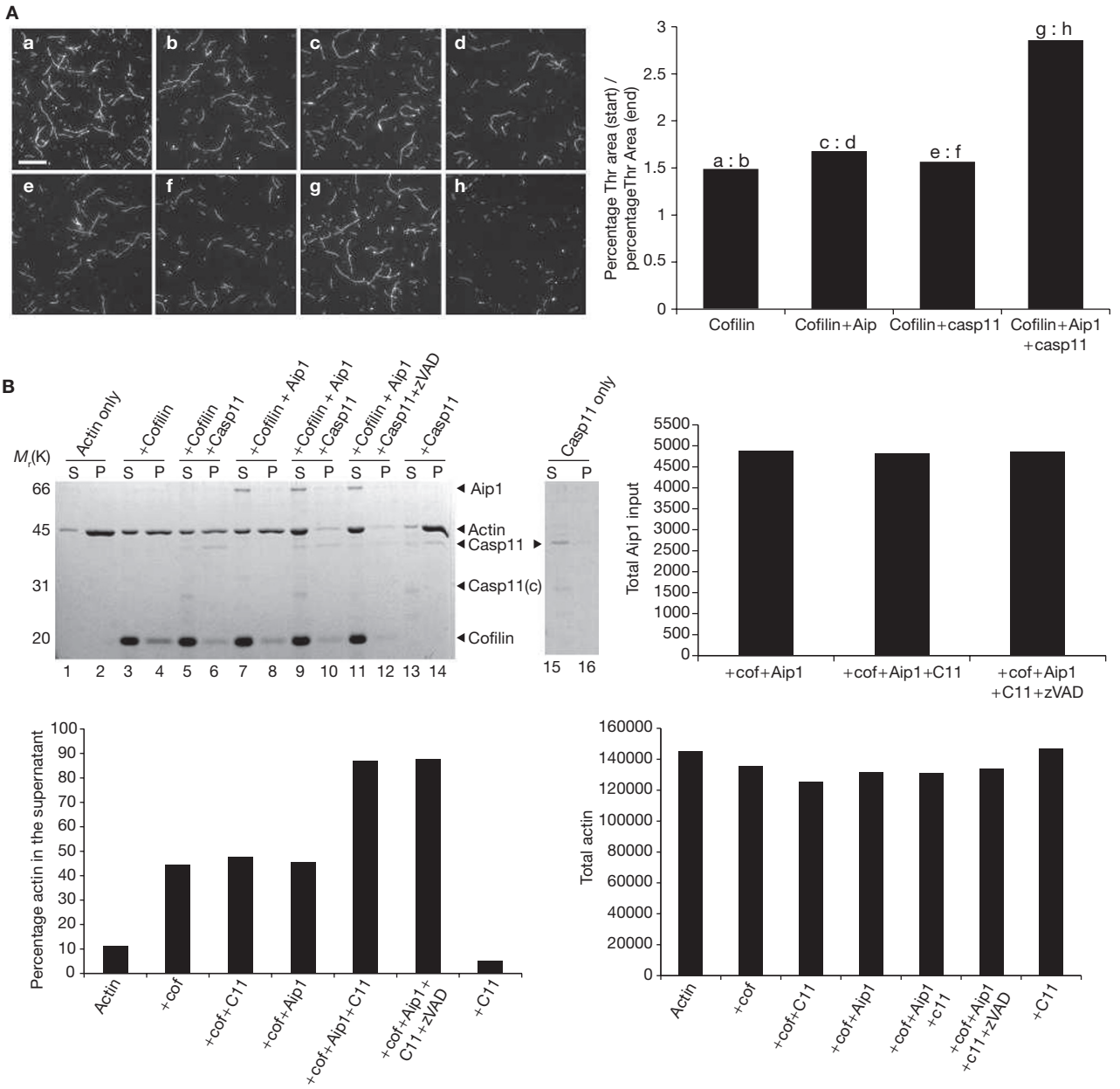

Figure 5 Caspase-11 regulates actin depolymerization *in vitro*. (**A**) Caspase-11 promotes cofilin- and Aip1-mediated actin depolymerization. *In vitro*-polymerized actin filament (1 μM; unlabelled actin monomer: Texas-red labelled actin monomer, 1:1) on filamin-coated glass slides was treated with cofilin (2 μM) alone (a, b), cofilin (2 μM) plus Aip1 (50 nM; c, d), cofilin (2 μM) plus caspase-11 (1 μM; e, f) or cofilin (2 μM) plus Aip1 (50 nM) plus caspase-11 (1 μM; g, h) for 5 min and random fields were photographed before (a, c, e, g) and after (b, d, f, h) treatment. Quantification of the fold change of the number of fluorescent filament pixels was calculated by the ratio of percentage of thresholded area before and after treatment. The scale bar represents 10 μm. (**b**) Caspase-11 and Aip1 cooperatively promote cofilin-dependent actin depolymerization. Actin monomers (4 μM) were polymerized *in vitro* for 1 h. Polymerized actin filaments (2 μM final concentration) were then incubated with cofilin (cof, 8 μM) alone or together with Aip1 (50 nM) or caspase-11 (C11, 1 μM) for 1 h and centrifuged at 109,000*g* for 20 min. F-actin pellet (P) and supernatant (S) were subjected to 12% SDS–PAGE followed by Gelcode-blue staining. Casp11(c), cleaved form of caspase-11. Total actin and Aip1 input (in arbitrary units) and the fraction of actin in the supernatant (percentage) were quantified.

cofilin and phospho-cofilin (p-cofilin) were compared in control and *Aip1* RNAi cells by western blotting (Fig. 6b and see Supplementary Information, Fig. S2d). Interestingly, compared with J774 psrp or J774 *Aip1*^{mut} RNAi1 cells, the levels of caspase-11 and cofilin were higher (1.92 ± 0.37-fold and 1.69 ± 0.25-fold, respectively, of *Aip1*^{mut} RNAi1), whereas p-cofilin (pSer 3; the inactive form of cofilin) levels were lower in J774 *Aip1* RNAi1 cells (0.211 ± 0.006-fold of *Aip1*^{mut} RNAi1), suggesting that reduced Aip1 expression in *Aip1* RNAi cells led to a compensatory upregulation of caspase-11 and cofilin functions. Further increase in cofilin levels in *Aip1* RNAi cells partially rescued the migration defect in *Aip1* RNAi cells (see Supplementary Information, Fig. S4a–c).

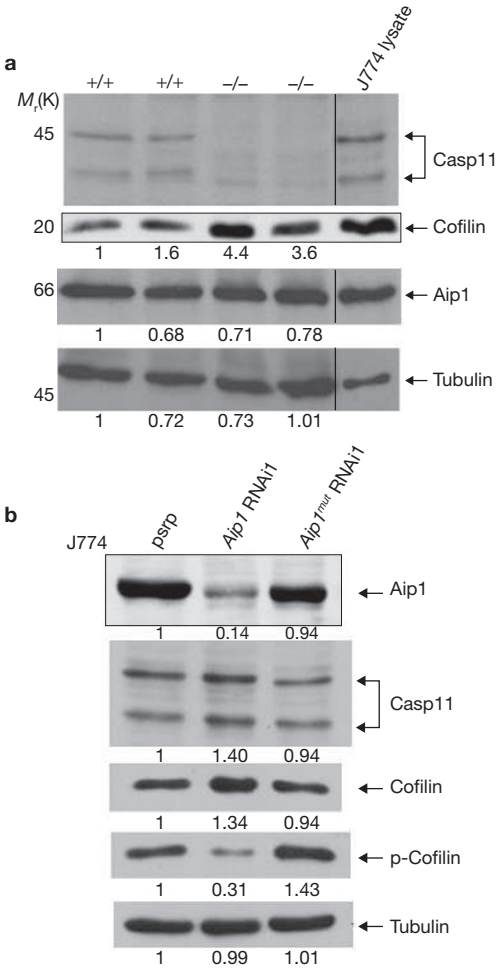

Figure 6 Cofilin levels are upregulated in *caspase-11*$^{-/-}$ spleen and *Aip1* RNAi cells. (**a**) The expression level of cofilin is upregulated in *caspase-11*$^{-/-}$ spleen. The western blots of lysates from flash-frozen spleen tissues of two wild-type (+/+) and two *caspase-11*$^{-/-}$ littermates were probed using anti-caspase-11, anti-Aip1 or anti-cofilin anti-bodies. J774 lysate served as a positive control. The band intensity was quantified by densitometry as a ratio to the first lanes. (**b**) The expression levels of cofilin, p-cofilin and caspase-11 in *Aip1* RNAi cells. The western blots of lysate from J774 vector control cells (psrp), *Aip1* RNAi cells and *Aip1*^{mut} RNAi1 control cells were probed with anti-caspase-11, anti-Aip1, anti-cofilin or anti-p-cofilin antibodies. The band intensity was quantified as in **a**.

The corresponding changes in gene expression in *caspase-11*$^{-/-}$ and *Aip1* RNAi cells described above reveal the attempts of cells to compensate for the loss of caspase-11 and Aip1 by regulating expression levels of cofilin and caspase-11, two proteins with previous unknown connection, and thus, provide evidence supporting a role for caspase-11 and Aip1 interaction in regulating cofilin-dependent actin depolymerization *in vivo*.

DISCUSSION

We propose a model for how caspase-11 may promote actin depolymerization (Fig. 7): caspase-11 may have an intrinsic affinity for F-actin (Fig. 5b). The N-terminal propeller of Aip1 is known to be critical for activating cofilin-mediated filament disassembly[14], whereas we show that the C-terminal WD40 propeller interacts with the CARD domain of caspase-11, similar to the CARD–WD40 interaction described in Apaf-1 (ref. 25), suggesting that the interaction between caspase-11 and the C-terminal propeller of Aip1 may help to recruit Aip1 to cofilin on F-actin.

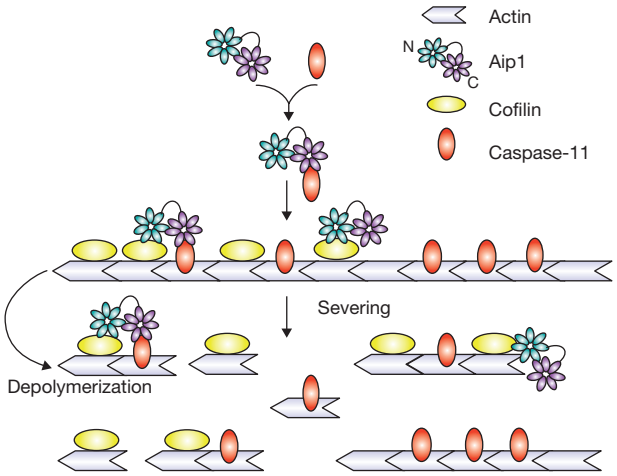

Figure 7 A schematic representation of a model for caspase-11-mediated cofilin- and Aip1-dependent actin depolymerization. The interaction of caspase-11 with F-actin and Aip1 increases the proximity of Aip1 to cofilin and F-actin to facilitate cofilin-mediated filament-severing activity, as well as to enhance depolymerization from the pointed ends.

The interaction of Aip1 with cofilin and F-actin-associated caspase-11 may facilitate cofilin-mediated filament severing activity and depolymerization (Fig. 7). We propose that, by regulating both the migration of cells involved in early host-defense response and cytokine secretion, the expression of caspase-11 may serve to deliver cytokine-producing cells to the site of infection in a rapid fashion, whereas apoptosis regulated by caspase-11 may function as an autoregulatory mechanism to terminate the cytokine release.

Our study demonstrates an unexpected role for caspase-11, a caspase known to be critical for cytokine secretion and apoptosis during inflammatory responses, in regulating cell migration. The interaction of caspase-11 with Aip1, a protein known to directly interact with the core machinery of the actin cytoskeleton, suggests that the normal physiological function of caspases may be much broader than their previously established roles in apoptosis and cytokine maturation. The ability of pro-inflammatory stimuli to regulate cell migration by upregulating the expression of caspase-11, an intracellular regulator of inflammatory response, provides a novel mechanism for cells to regulate migration in a manner very different from that of receptor-mediated, PI(3)K–Rac–Rho-regulated cytoskeleton reorganization. Finally, as actin dynamics are involved in regulating multiple cellular events (including cell migration, cell division and secretion), the ability of caspase-11 to regulate actin depolymerization may provide a potential mechanism for caspase-11-mediated control of additional events during inflammatory responses. □

METHODS

Flag-tagged affinity purification and mass spectrometry. Forty 15-cm plates of J774 cells (~2 × 10^8 cells) were treated with LPS (2 μg ml^{-1}) for 10 h and then lysed in immunoprecipitation (IP) lysis buffer (50 mM HEPES–KOH at pH 7.4, 150 mM NaCl, 1 mM EDTA, 0.1% NP40, 10% glycerol). The cell extract was mixed with M2 agarose beads (Sigma, St Louis, MO) for 6 h and then loaded onto the column. The column was then washed extensively with IP lysis buffer and eluted with IP lysis buffer containing 0.5 mg ml^{-1} Flag peptide (Sigma). The eluate was further concentrated with Centricon YM-3 centrifugal filter devices (Millipore, Billerica, MA) and separated by SDS–PAGE. The gel was stained by Gelcode blue (Pierce, Rockford, IL) and a unique 66K band in the caspase-11

sample lane, as well as the corresponding region in the control lane, were cut out for mass spectrometry analysis by the Taplin Biological Mass Spectrometry Facility at Harvard Medical School (Boston, MA). Two peptides specific for mouse Aip1 (NIDNPAIADIYTEHAHQVVVAK and VYSILASTLKDEGK) were only recovered in the caspase-11 sample lane, but not in the control lane.

Homing assay. Splenocytes from wild-type and *caspase-11*$^{-/-}$ mice were labelled for 20 min with tetramethylrhodamine-5-isothiocyanate (TRITC, 30 μg ml^{-1}; Molecular Probes, Carlsbad, CA) and 5-(and-6)-carboxyfluorescein diacetate, succinimidyl ester (CFSE, 20 μg ml^{-1}; Molecular Probes) at 37 °C. The cells were centrifuged in FBS to remove dead cells and excess dye. Equal numbers (5×10^7) of splenocytes from each genotype were mixed and injected intravenously into three recipient wild-type mice. An aliquot of the input was saved for later FACS analysis to control for variability in the relative frequency of transferred TRITC$^+$ ($[\text{TRITC}]_{\text{input}}$) and CSFE$^+$ ($[\text{CSFE}]_{\text{input}}$) populations. After 1 h, recipient mice were killed by CO_2 and blood was collected by cardiac puncture. Bone marrow was obtained by flushing through the femur and tibia. Spleens, PLNs, MLNs and Peyer's patches were harvested and passed through wire mesh. Single-cell suspensions were further stained with APC-labelled anti-CD4 and PerCP-labelled anti-B220 (BD biosciences, San Jose, CA) and analysed by four-colour flow cytometry. Homing index = $\text{TRITC}^+ \%_{\text{organ}} / \text{CSFE}^+ \%_{\text{organ}} : \text{TRITC}^+ \%_{\text{input}} / \text{CSFE}^+ \%_{\text{input.}}$

***In vitro* differentiation of T cells and peritonitis induction**. The *in vitro* differentiation of T cells and peritonitis induction protocol developed by Goodarzi *et al.*[13] was followed. Briefly, splenocytes isolated from wild-type and *caspase-11*$^{-/-}$ mice were stimulated with anti-CD3ε (1 μg ml^{-1}) for 48 h. Subsequently, cells were washed and incubated in media containing 20 ng ml^{-1} IL-2 for 8–10 days to differentiate into T effector cells. Before each experiment, the activation phenotype was assessed by flow cytometric analysis of cell size, CD25, CD44 and L-selectin. IL-2-treated cell populations contained >90% CD8$^+$ T cells and L-selectin^{low}CD25^{hi}CD44^{hi} (see Supplementary Information, Fig. S4d).

To induce peritonitis, emulsified complete Freund's adjuvant (CFA) in PBS (0.5 ml 1:1 dilution, volume:volume) was intraperitoneally injected into wild-type C57BL/6J mice. At 3 days after induction of peritonitis, effector T cells were fluorescently labelled as described for the homing assay protocol and injected into recipient mice through tail veins. After 20 h, recipient mice were killed and blood, spleen, peripheral and mesenteric lymph nodes, liver and lung were collected. PELs were collected from the peritoneal cavity by lavage with PBS. Liver and lung tissues were digested with collagenase type 2 (0.5%; Worthington Biochemical, Lakewood, NJ) at 37 °C for 20 min before passing through wire mesh. Single-cell suspensions were stained with anti-CD8, and the ratio of homed wild-type to *caspase-11*$^{-/-}$ CD8$^+$ T cells in each organ was analysed by flow cytometry.

Measurement of fMLP-induced membrane ruffling and actin staining. J774 cells (5×10^4) were plated on glass coverslips in 24-well plates in DMEM with 10% FBS overnight. Adherent cells were washed twice with serum free DMEM media and serum starved for 1 h. fMLP (100 nM) was added to cells. The cells were fixed after 30 s, 1 min, 2 min, 5 min and 10 min stimulation, by the addition of 4% formaldehyde, and then incubated for an additional 15 min. After permeabilization in 0.1% Triton–PBS for 5 min, cells on coverslips were blocked with 1%BSA in PBS for another 20 min. F-actin structure was visualized by staining with rhodamine–phalloidin (1:100 dilution, Molecular Probes) for 30 min. Images were taken using a Nikon E800 fluorescence microscope with a 40× objective. The ruffling index was calculated according to Cox *et al.*[17] with minor modifications. Ruffling was defined by the presence of F-actin-rich submembranous folds using fluorescence microscopy. The extent of ruffling in each cell was scored using a scale of 0–2, where 0 indicates that no ruffles were present, 1 indicates that ruffling was confined to one area of the cell only (or <50% of the cell's circumference), and 2 indicates that two or more discrete areas (and >50% of the cell's circumference) of the cell contained ruffling. The ruffling index was recorded as the sum of the ruffling scores of 100 cells.

Single actin-filament depolymerization assay. Unlabelled G-actin (10 μM) and 10 μM Texas-red labelled actin were mixed and polymerized in Buffer A (50 mM KCl, 2 mM $MgCl_2$, 2 mM ATP, 20 mM PIPES at pH 6.8 and 10 mM β-mercaptoethanol) for 1 h at room temperature. A 0.1% nitrocellulose-coated coverslip was mounted onto a slide glass with two pieces of double-sided sticky tape to make a perfusion chamber. Filamin (1 μM) in buffer B (100 mM HEPES at pH 7.4, 50 mM KCl, 2 mM $MgCl_2$) was perfused into the chamber and incubated for 10 min. After the chamber was washed twice with buffer B, casein (5 mg ml^{-1}) was perfused into the chamber for blocking. Polymerized actin filaments were diluted tenfold in anti-bleaching buffer (buffer B containing 0.036 mg ml^{-1} catalase, 0.2 mg ml^{-1} glucose oxidase, 6 mg ml^{-1} glucose and 10 mM β-mercaptoethanol) and perfused into the chamber. After 10 min, the chamber was washed twice with anti-bleaching buffer and two random images were taken under Nikon 90i upright fluorescent microscope (60× objective) and a Hamamatsu Orca-ER CCD camera. Polymerized actin filaments were then treated with different combinations of purified human cofilin, bovine Aip1 and His-tagged recombinant caspase-11 for 5 min. The chamber was washed with anti-bleaching buffer and another two random images were taken from the same sample slide. Each image contained 600–900 individual fluorescent filaments. The quantity of fluorescent filament pixels was indicated by percentage thresholded area (the background fluorescence reading is the threshold value.).

Actin-pelleting assay. The actin-pelleting assay protocol[24] was adapted with minor modifications. Briefly, 4 μM actin was polymerized at room temperature in F-buffer (5 mM Tris at pH 7.5, 0.7 mM ATP, 0.2 mM $CaCl_2$, 2 mM $MgCl_2$, 100 mM KCl and 1 mM DTT). After 1 h, polymerized actin (final concentration, 2 μM) was added to different concentrations of cofilin, Aip1 or caspase-11 in F-buffer. The reactions were incubated at room temperature for 1 h and centrifuged at 109,000*g* for 20 min at 23 °C in a TLA100 rotor (Beckman Instruments, Fullerton, CA). Equal proportions of the pellets and supernatants were run on 12% SDS–PAGE, and proteins were visualized by Gelcode blue staining (Pierce Biotechnology).

Note: Supplementary Information is available on the Nature Cell Biology website.

ACKNOWLEDGEMENTS

We thank Q. Shi and R. King for kindly allowing us to use the time-lapse microscope setup and J. Waters in the Nikon Imaging Center of Harvard Medical School for expert help with cell imaging. We thank C. Mahlke for mouse genotyping. We thank M. Boyce, A. Degterev, M. Lipinski and R. Sanchez-Olea for critical reading of this manuscript and members of Yuan laboratory for helpful suggestions during the course of this work. This work was supported in part by a NIH Merit Award (R37 AG12859 to J. Y.).

AUTHOR CONTRIBUTIONS

J.L. identified Aip1 as a caspase-11 binding protein, and discovered and characterized the defects of *caspase-11*$^{-/-}$ cells in migration. W.B. and J.L. performed the *in vitro* actin depolymerization assays. L.S. and J.L. performed the *in vivo* homing assay. S.J.K. and J.L. examined the composition of *caspase-11*$^{-/-}$ immune system. H.Z. generated anti-Aip1 antibodies. J.L. and J.Y. wrote the paper. J.Y. directed the work. All authors discussed the results and commented on the manuscript.

COMPETING FINANCIAL INTERESTS

The authors declare that they have no competing financial interests.

Published online at http://www.nature.com/naturecellbiology/
Reprints and permissions information is available online at http://npg.nature.com/reprintsandpermissions/

1. Cryns, V. & Yuan, J. Proteases to die for. *Genes Dev.* **12,** 1551–1570 (1998).
2. Wang, S. *et al.* Identification and characterization of Ich-3, a member of the interleukin-1β converting enzyme (ICE)/Ced-3 family and an upstream regulator of ICE. *J. Biol. Chem.* **271,** 20580–20587 (1996).
3. Wang, S. *et al.* Murine caspase-11, an ICE-interacting protease, is essential for the activation of ICE. *Cell* **92,** 501–509 (1998).
4. Kang, S. J. *et al.* Dual role of caspase-11 in mediating activation of caspase-1 and caspase-3 under pathological conditions. *J. Cell Biol.* **149,** 613–622 (2000).
5. Kang, S. J., Wang, S., Kuida, K. & Yuan, J. Distinct downstream pathways of caspase-11 in regulating apoptosis and cytokine maturation during septic shock response. *Cell Death Differ.* **9,** 1115–1125 (2002).
6. Pollard, T. D. & Borisy, G. G. Cellular motility driven by assembly and disassembly of actin filaments. *Cell* **112,** 453–465 (2003).
7. Bamburg, J. R. Proteins of the ADF/cofilin family: essential regulators of actin dynamics. *Annu. Rev. Cell Dev. Biol.* **15,** 185–230 (1999).
8. Ono, S. Regulation of actin filament dynamics by actin depolymerizing factor/cofilin and actin-interacting protein 1: new blades for twisted filaments. *Biochemistry* **42,** 13363–13370 (2003).
9. Okada, K. *et al. Xenopus* actin-interacting protein 1 (XAip1) enhances cofilin fragmentation of filaments by capping filament ends. *J. Biol. Chem.* **277,** 43011–43016 (2002).

10. Konzok, A. *et al.* DAip1, a *Dictyostelium* homologue of the yeast actin-interacting protein 1, is involved in endocytosis, cytokinesis, and motility. *J. Cell Biol.* **146,** 453–464 (1999).
11. Geisbrecht, E. R. & Montell, D. J. A role for *Drosophila* IAP1-mediated caspase inhibition in Rac-dependent cell migration. *Cell* **118,** 111–125 (2004).
12. Weninger, W., Crowley, M. A., Manjunath, N. & von Andrian, U. H. Migratory properties of naive, effector, and memory CD8(+) T cells. *J. Exp. Med.* **194,** 953–966 (2001).
13. Goodarzi, K., Goodarzi, M., Tager, A. M., Luster, A. D. & von Andrian, U. H. Leukotriene B4 and BLT1 control cytotoxic effector T cell recruitment to inflamed tissues. *Nature Immunol.* **4,** 965–973 (2003).
14. Mohri, K., Vorobiev, S., Fedorov, A. A., Almo, S. C. & Ono, S. Identification of functional residues on *Caenorhabditis elegans* actin-interacting protein 1 (UNC-78) for disassembly of actin depolymerizing factor/cofilin-bound actin filaments. *J. Biol. Chem.* **279,** 31697–31707 (2004).
15. Yang, L. V., Radu, C. G., Wang, L., Riedinger, M. & Witte, O. N. Gi-independent macrophage chemotaxis to lysophosphatidylcholine via the immunoregulatory GPCR G2A. *Blood* **105,** 1127–1134 (2005).
16. Southwick, F. S., Dabiri, G. A., Paschetto, M. & Zigmond, S. H. Polymorphonuclear leukocyte adherence induces actin polymerization by a transduction pathway which differs from that used by chemoattractants. *J. Cell Biol.* **109,** 1561–1569 (1989).
17. Cox, D. *et al.* Requirements for both Rac1 and Cdc42 in membrane ruffling and phagocytosis in leukocytes. *J. Exp. Med.* **186,** 1487–1494 (1997).
18. Rogers, S. L., Wiedemann, U., Stuurman, N. & Vale, R. D. Molecular requirements for actin-based lamella formation in *Drosophila* S2 cells. *J. Cell Biol.* **162,** 1079–1088 (2003).
19. Cramer, L. P. Role of actin-filament disassembly in lamellipodium protrusion in motile cells revealed using the drug jasplakinolide. *Curr. Biol.* **9,** 1095–1105 (1999).
20. Dawe, H. R., Minamide, L. S., Bamburg, J. R. & Cramer, L. P. ADF/cofilin controls cell polarity during fibroblast migration. *Curr. Biol.* **13,** 252–257 (2003).
21. Heyworth, P. G., Robinson, J. M., Ding, J., Ellis, B. A. & Badwey, J. A. Cofilin undergoes rapid dephosphorylation in stimulated neutrophils and translocates to ruffled membranes enriched in products of the NADPH oxidase complex. *Histochem. Cell Biol.* **108,** 221–233 (1997).
22. Bleul, C. C., Fuhlbrigge, R. C., Casasnovas, J. M., Aiuti, A. & Springer, T. A. A highly efficacious lymphocyte chemoattractant, stromal cell-derived factor 1 (SDF-1). *J. Exp. Med.* **184,** 1101–1109 (1996).
23. Fujibuchi, T. *et al.* AIP1/WDR1 supports mitotic cell rounding. *Biochem. Biophys. Res. Commun.* **327,** 268–275 (2005).
24. Rodal, A. A., Tetreault, J. W., Lappalainen, P., Drubin, D. G. & Amberg, D. C. Aip1p interacts with cofilin to disassemble actin filaments. *J. Cell Biol.* **145,** 1251–1264 (1999).
25. Ferraro, E., Corvaro, M. & Cecconi, F. Physiological and pathological roles of Apaf1 and the apoptosome. *J. Cell. Mol. Med.* **7,** 21–34 (2003).
26. Brieher, W. M., Coughlin, M. & Mitchison, T. J. Fascin-mediated propulsion of *Listeria monocytogenes* independent of frequent nucleation by the Arp2/3 complex. *J. Cell Biol.* **165,** 233–242 (2004).
27. Maciver, S. K., Pope, B. J., Whytock, S. & Weeds, A. G. The effect of two actin depolymerizing factors (ADF/cofilins) on actin filament turnover: pH sensitivity of F-actin binding by human ADF, but not of *Acanthamoeba actophorin*. *Eur. J. Biochem.* **256,** 388–397 (1998).
28. Brieher, W. M., Kueh, H. Y., Ballif, B. A. & Mitchison, T. J. Rapid actin monomer-insensitive depolymerization of *Listeria* actin comet tails by cofilin, coronin, and Aip1. *J. Cell Biol.* **175,** 315–324 (2006).

nature cell biology

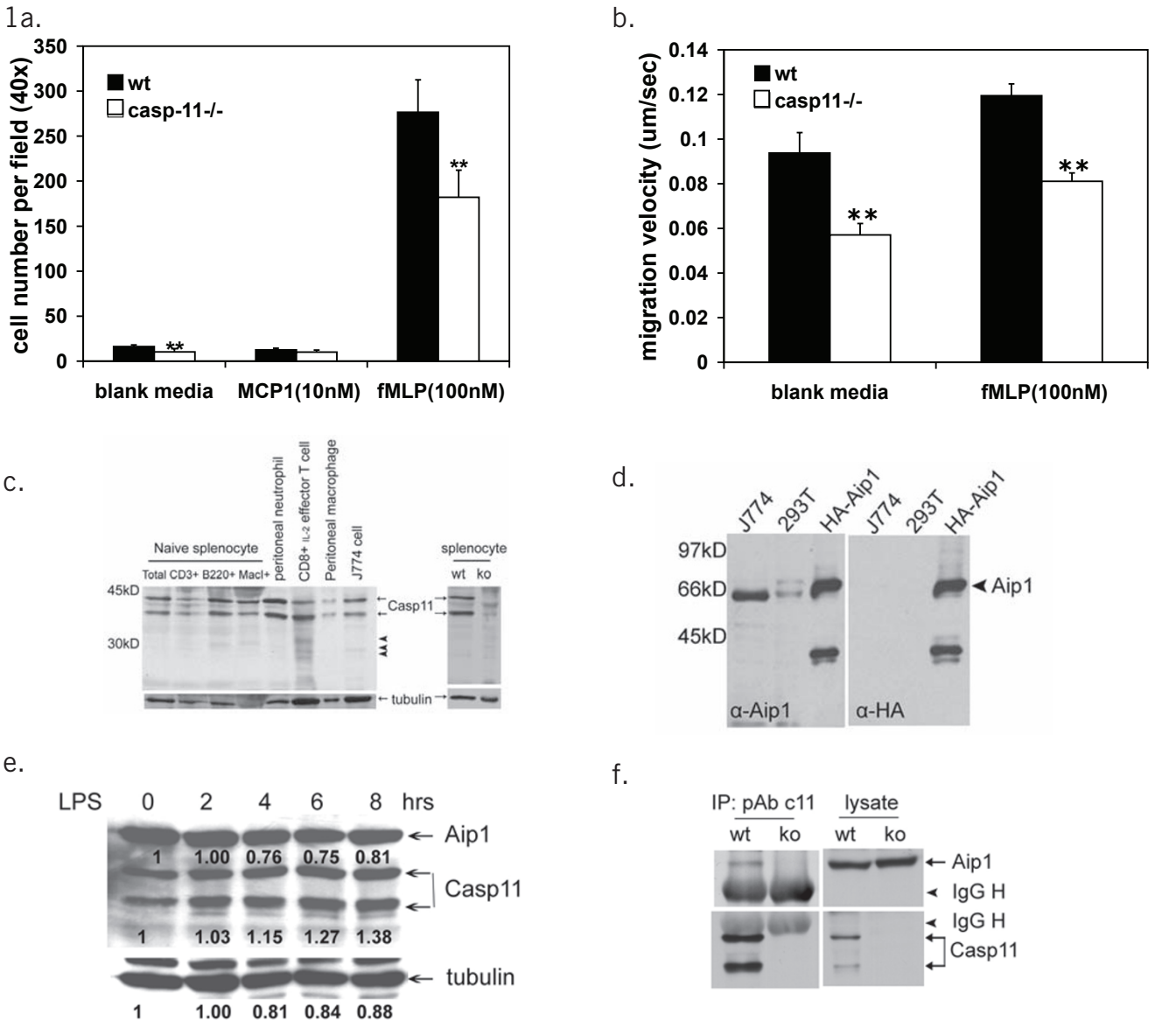

Figure S1 (a) Transwell migration of control and caspase-11-/- neutrophils. Details see methods. ** p<0.01. **(b)** An analysis of caspase-11-/- peritoneal neutrophil migration using time-lapse microscopy. Details see methods. Error bar: s.e.m. of the migration velocity of 20 cells of each genotype. ** p<0.01. **(c)** An analysis of caspase-11 expression profile in leukocytes. T cells ($CD3^+$), B cells ($B220^+$) and macrophages ($MacI^+$) from spleens of naïve unstimulated mice were purified by FACS. The western blot of the cell lysates was probed with anti-caspase-11 monoclonal antibody. wt, wild type control splenocytes; ko, caspase-11-/- splenocytes. **(d)** Anti-Aip1 monoclonal antibody recognizes both endogenous and transfected mouse Aip1. The western blots of cell lysates from J774 cells, 293T cells and 293T cells transfected with HA-tagged mouse Aip1 were probed with anti-Aip1 monoclonal antibody or anti-HA antibody. **(e)** A temporal analysis of caspase-11 and Aip1 expression levels in LPS treated J774 cells. J774 cells were treated with 2μg/ml LPS for indicated time. The western blots of cell lysates were probed with anti-Aip1 and anti-caspase-11 monoclonal antibodies. Protein levels were measured by densitometry and normalized according to the first lane. **(f)** Interaction of endogenous caspase-11 and Aip1 in wt splenocytes. The splenocytes from two control and two caspase-11-/- mice were pooled. Total lysates were immunoprecipitated with anti-caspase-11 rabbit polyclonal antibody (pAb c11, as in Fig. 2e). The western blots of immunocomplexes and the lysate input were probed with rat anti-Aip1 monoclonal antibody or rat anti-caspase-11 monoclonal antibody. wt, caspase-11+/+; ko, caspase-11-/-.

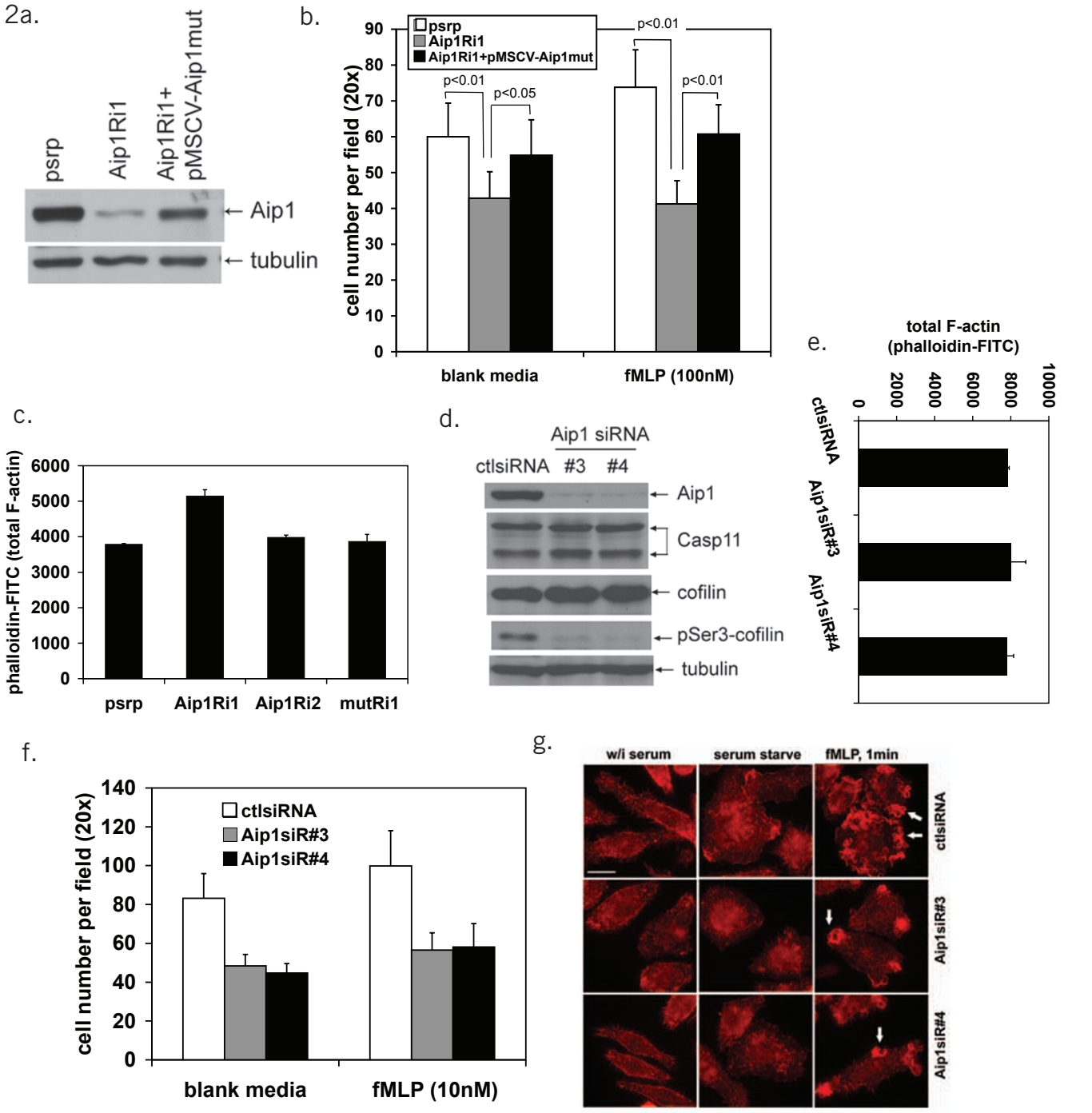

Figure S2 (a) The cDNA of Aip1 open reading frame was mutated at nucleotide 279 position (T → G) andsubcloned into pMSCV-neo retroviral vector. Aip1 Ri1 cells were infected with retrovirus carrying mutated Aip1 cDNA (pMSCV-Aip1mut) and selected with 300μg/ml G418 for three days (non-infected Aip1Ri1 cells all died by three days). The western blots of cell lysates of control psrp cells, Aip1Ri1 cells and Aip1Ri1 cells stably expressing pMSCV-Aip1mut (Aip1Ri1+pMSCV-Aip1mut) were probed with anti-Aip1 and anti-tubulin antibodies. **(b)** Migration of control psrp, Aip1Ri1 and Aip1Ri1 stably expressing pMSCV-Aip1mut toward blank media and fMLP (100nM) was measured in a transwell migration assay in Fig 3b. **(c)** Quantification of total F-actin amount in J774 psrp vector control and Aip1 RNAi stable cells. $6x10^4$ cells were seeded in 24 well plate overnight. F-actin was labeled with phalloidin-FITC. Total phalloidin-FITC incorporated was extracted by methanol and fluorescence was measured at F_{exc}485nm/ F_{emi}535nm. Error bars represent s.d. of triplicate wells. **(d)** Transient knockdown of Aip1 in J774 cells by synthetic siRNA oligos. Two synthetic siRNA oligos (Aip1siR #3 & #4) knocked down the expression of endogenous Aip1 in J774 cells. siRNA oligos (Dharmacon) were electroporated into J774 cells using Amaxa Nucleofector machine. The protein level was measured 48h post transfection. **(e)** Quantification of total F-actin amount in transient Aip1 knockdown cells. The experimental procedure was as in (**c**). **(f)** Migration of transient Aip1 knockdown cells toward blank media and fMLP (10nM). The experimental procedure was as in Fig 3b. **(g)** Membrane ruffling formation in fMLP (10nM) stimulated J774 control and transient Aip1 knockdown cells. The experimental procedure was as in Fig 3c. Scale bar represents 18μm.

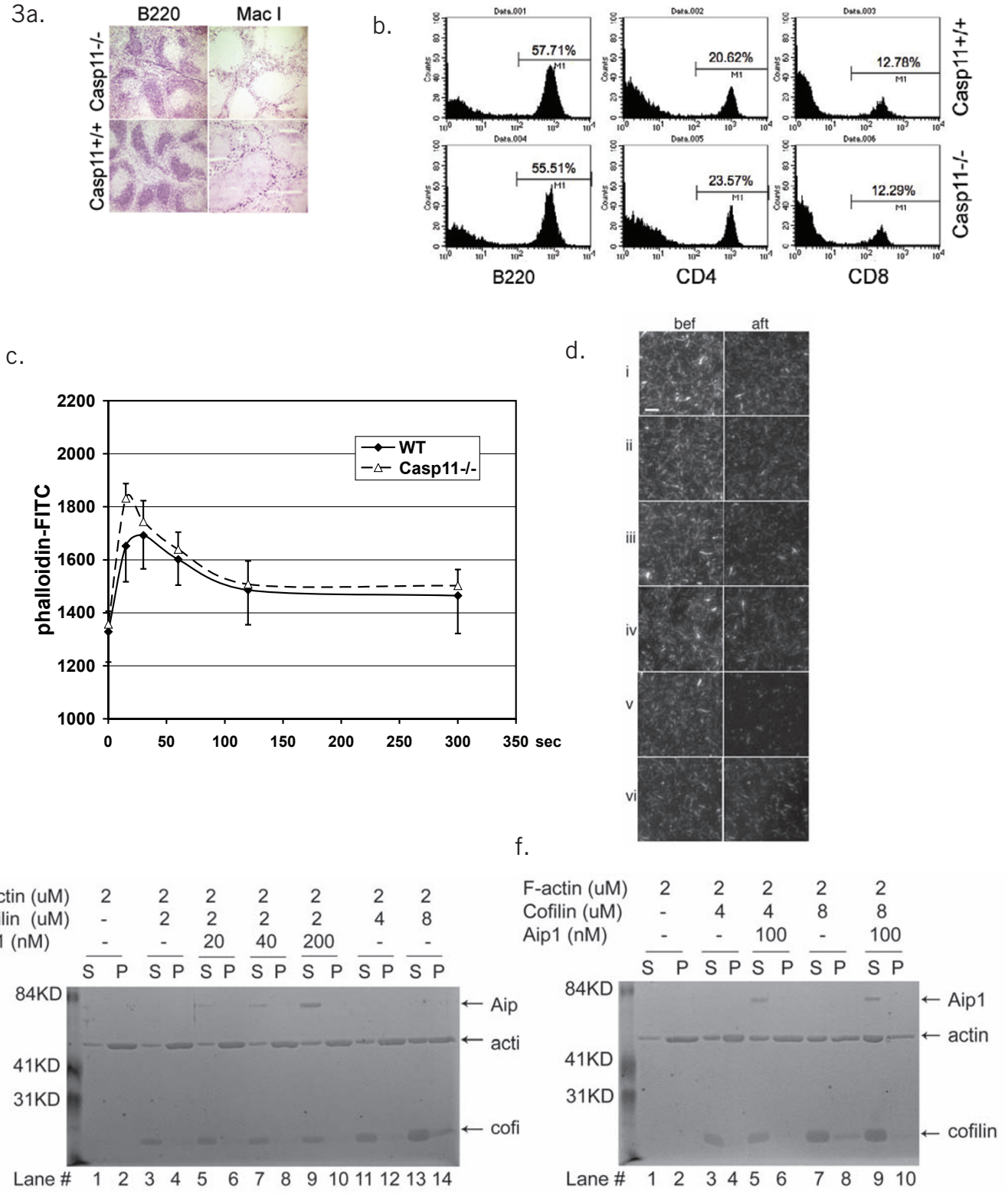

Figure S3 (a) Immunohistochemistry of spleen sections from control and caspase-11-/- mice by anti-B220 and anti-MacI staining. **(b)** FACS analysis of splenocyte composition by anti-B220-PE (B cells), anti-CD4-PE (CD4 T cells) and anti-CD8-PE (CD8 T cells) staining. **(c)** The experimental procedure was as in Fig 4c. Absolute value of phalloidin-FITC reading is shown on the y-axis here. The curves are from mean±s.e.m of phalloidin-FITC from 4 experiments. **(d)** The experimental procedure was as in Fig 5a, except that the images were taken from the same field before (bef) and after (aft) each treatment. (i), cofilin (2μM); (ii), cofilin (2μM) and Aip1 (50nM); (iii), cofilin (2μM) and Aip1 (100nM); (iv), cofilin (2μM) and caspase-11 (1μM); (v), cofilin (2μM) and Aip1 (50nM) and caspase-11 (1μM); (vi), caspase-11 (1μM). Scale bar represents 3.6μm. **(e&f)** Aip1 promotes cofilin-dependent actin depolymerization in pelleting assay. The experimental procedure was as in Fig 5b. S, supernatant; P, pellet.

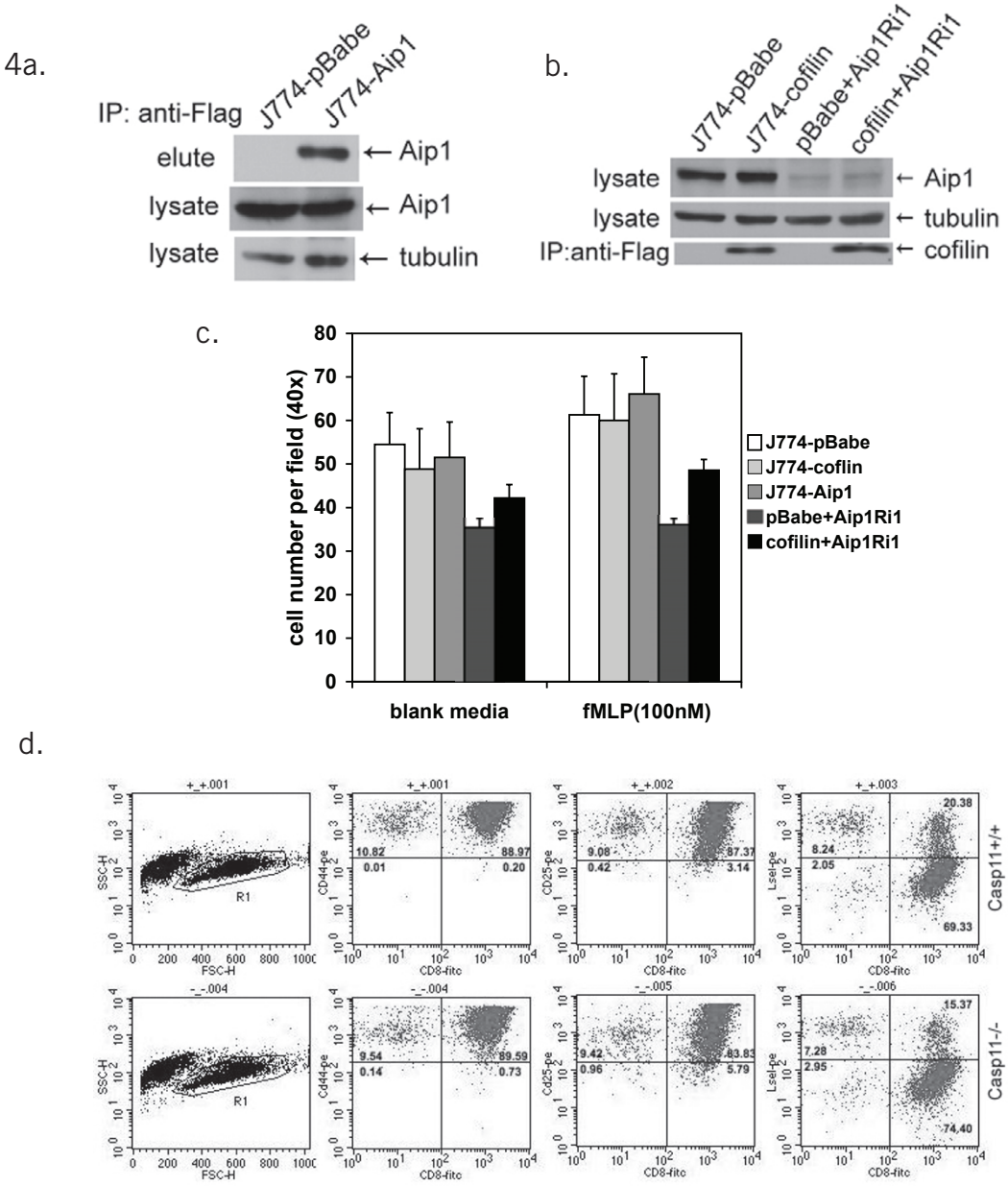

Figure S4 (a) The expression levels of Aip1 and cofilin in J774-cofilin and J774-Aip1 stable cells. J774 cells stably expression Flag-cofilin and Flag-Aip1 (J774-cofilin and J774-Aip1) were made by infecting J774 cells with retrovirus carrying pBabe-Flag-cofilin and pBabe-Flag-Aip1 vectors and selected in 2μg/ml puromycin for 2 weeks. The cell lysate was immunoprecipitated with anti-Flag M2 bead. The western blots of lysate and immunocomplex were probed with anti-Aip1 and anti-cofilin antibodies. **(b)** Knockdown of Aip1 in control stable cells (pBabe+Aip1Ri1) and Flag-cofilin expressing stable cells (cofilin+Aip1Ri1). J774-pBabe and J774-cofilin cells were infected with Aip1 RNAi1 virus twice without puromycin selection (because both pBabe and Aip1 RNAi vector psrp carry puromycin selection marker). Aip1 and cofilin expression levels in parental cells (J774-pBabe and J774-cofilin) and RNAi cells (pBabe+Aip1Ri1 and cofilin+Aip1Ri1) were shown by western blots. **(c)** Transwell migration of cofilin and Aip1 stable cells as well as Aip1RNAi cells. The experimental procedure was similar to that in Fig 3f except that cells were counted using 40x objective. **(d)** *In vitro* differentiated $CD8^{IL\text{-}2}$ effector T cells were stained with anti-CD8, anti-CD44, anti-CD25 and anti-L-selectin antibodies for testing the differentiation efficiency before they were used in the homing assay in Fig. 1d & 1e.

(Methods in SI)

Methods

Mice and reagents

Eight to twelve weeks old caspase-11-/- mice, which had been backcrossed to C57BL/6J for 8 times[3] and the control littermates (wt) were used for this study. Antibodies used: anti-caspase-11 rat monoclonal and rabbit polyclonal antibodies[3], anti-HA (Covance), anti-cofilin (Santa Cruz) and anti-pSer3-cofilin (Cell Signaling). Anti-FLAG M2 agarose beads were from Sigma. Anti-HA agarose beads were from Santa Cruz Biotechnology. LPS was from Sigma. fMLP was from Calbiochem. Mouse MCP1, SDF1α, SLC and BLC were from R & D systems.

Generation of J774 stable cell lines expressing FLAG-tagged caspase-11(C254G), Aip1 and cofilin

PCR fragments of the ORF of cDNAs encoding mutant caspase-11(C254G), mouse Aip1 (IMAGE clone ID: 6812096, ATCC) and mouse cofilin1 (IMAGE clone ID: 6820355, ATCC) were inserted into EcoRI and SalI sites of pBabe-FLAG-puro retroviral vector. Virus was made in 293T cells for infection of J774 cells. Cells were selected by puromycin (2 μg/ml) for two weeks before experiments.

Generation of anti-Aip1 monoclonal antibody

Mouse Aip1 cDNA (IMAGE clone ID: 6812096, ATCC) was PCR amplified and subcloned into His-tagged bacteria expression vector pET28a. His-tagged Aip1 construct was transformed into BL21(DE3) cells. Bacteria were cultured until OD_{600}=0.8-1 and

induced with 0.3mM IPTG for 3 hours. Recombinant His-tagged Aip1 protein was purified with Ni-NTA agarose beads (Qiagen). The anti-Aip1 monoclonal antibody was isolated from rats immunized with recombinant His-tagged Aip1 protein.

Construction of Aip1 and Caspase-11 truncation mutants

Full length Aip1 (aa.1-602), the N-terminal propeller of Aip1 (aa.10-322) and the C-terminal propeller without the N-terminal first β strand (C-; aa.317-602) were PCR amplified from the mouse Aip1 cDNA image clone (ID: 6812096) and inserted into pCDNA3-HA vector at EcoRI/NotI sites. The C-terminal propeller with the N-terminal first β strand (C+; aa.317-602 plus aa.1-10) was PCR amplified with primer sets: 5'-ggggaattcaagggtcacagtaaatc-3'(forward primer) and 5'-ggggcggccgcttaggcgaacaccttctt-gatctcgtacggcatgtaggtgattgtcc-3' (reverse primer) from the C- construct and inserted into pCDNA3-HA vector at EcoRI/NotI sites.

The cDNAs coding for the full length caspase-11 (aa.1-374), p30 (aa.81-374) and the CARD (aa.1-98) were PCR amplified from the caspase-11 cDNA template pJ667 (ref4) and inserted into p3XFLAG-CMV vector at EcoRI/BamHI sites.

Capase-11 RNAi in J774 cells

Synthesized siRNA oligos targeting caspase-11 (siGENOME set of 4 duplex) and non-targeting control oligos were purchased from Dharmacon. siRNA oligos were electroporated into J774 cells using Amaxa Nucleofector machine according to the manufacturer's protocol. Caspase-11 level was measured by western blot 48 h after transfection.

Aip1 RNAi in J774 cells

Oligonucleotides corresponding to the sense 5'-ggagcatcttctaaagtat-3' and anti-sense 5'-atactttagaagatgctcc-3' (Ri1), sense 5'-ggtggtcacagtattcagt-3' and anti-sense 5'-actgaatactgtgaccacc-3' (Ri2) for mouse Aip1 were annealed and inserted into pSRP-puro vector at BglII/XhoI sites. pSRP-Aip1 RNAi or pSRP vector plasmid was transfected into 293T cells for retrovirus production. J774 cells were infected with the virus and selected with puromycin (2μg/ml) for two weeks. The sequences of point mutant RNAi construct (mutRi1) are 5'-ggagcatctgctaaagtat-3' (sense) and 5'-atactttagcagatgctcc-3' (anti-sense).

Protein purification

Monomer actin purification and labeling was as described in Brieher et al.[26]. Human cofilin-1 purification was as described in Maciver et al.[27]. Aip1 was purified from bovine thymus as described in Brieher et al.[28]. His-tagged caspase-11 purification was described in Kang et al.[4].

Transwell migration assay

Splenocytes (10^6) were loaded onto the inserts of a 24 well transwell plate (5μm pore size, Costar). Blank media and different concentration of chemokines were loaded into the bottom wells. After 2 hours, cells migrated into the bottom wells were collected by vigorous pipetting and counted by FACS. For J774 cells, 10^5 cells were added onto the inserts of an 8 μm pore size transwell plate and equilibrated in culture incubator for 30 min. Chemokines were then added to the bottom well. After 2 hours, cells on the

inserts were fixed with 4% paraformaldehyde for 20 min. Cells on the top surface of the insert were wiped off with a cotton swab. Cells on the bottom surface of the insert were stained with Hoechst dye and counted at nine random fields under Nikon TE300 inverted fluorescent microscope (20x objective). For neutropil migration, peritoneal neutrophils were isolated from the peritoneal lavage of 4 hr thioglycollate-stimulated control and caspase-11-/- mice. 10^5 peritoneal leukocytes were seeded on each of the 24 well transwell inserts (3μm pore size, Costar). After 1hr, the transwell insert were fixed and stained with anti-Gr1-FITC and anti-CD11b-PE antibodies. The cells on the top surface of the insert were scraped off with cotton swab. $Gr1^+CD11b^+$ cells on the bottom surface of the transwell insert were counted using a 40x objective. The cell numbers were corrected according to the ratio of % $Gr1^+CD11b^+$ in the input cells.

Time-lapse microscopy of peritoneal macrophage migration

Mice were injected with 1ml 4% thioglycollate media (Sigma) and 4 days later, cells from peritoneal exudate were collected and seeded onto four-well chamber slides (LAB-TEK, Nalge Nunc International). After 3 hours, unattached cells were washed away and the attached cells are mainly macrophages. Cells were around 50%-60% confluent and incubated overnight before imaging. Chamber slides were put on a Nikon TE2000E inverted microscope fitted with a Hamamatsu Orca-ER CCD camera with 37°C heated work station and humidified 5% CO_2 supply. Images were taken every 8 minutes for 20 hours with a 20x DIC objective. Migration velocity was calculated with the Metamorph software (Universal Imaging) by tracing individual cell nuclei movement over 50 frames.

For peritoneal neutrophil migration, ~$4x10^5$ freshly isolated peritoneal neutrophils were seeded on each of 35mm glass bottom microwell dishes (MatTek). The dishes were pre-coated with 5μg human fibronectin. After seeding for 30min, floating cells were washed away. The remaining cells were cultured in blank media or with 100nM fMLP. The images were taken at 30 sec interval for 20 min. The migration velocity was calculated by total distance of cell body movement / total time (40 frames).

F-actin measurement by phalloidin labeling

SDF-1α was added into splenocyte suspension at the final concentration of 100 ng/ml. At different time point (15s, 30s, 1min, 2min, 5min) after SDF-1α addition, an aliquot of cell suspension (~ $5x10^6$) was added to equal volume of 8% paraformaldehyde and fixed for 15 min. After washing twice with PBS, cells were permeabilized with 0.1% Triton for 5 min and then labeled with phalloidin-FITC (0.165μM in PBS/5% FBS; Molecular Probes) for 20 min. After washed with PBS, cells were resuspended in 1ml PBS/5%FBS and analyzed by flow cytometry (FACScan, Becton Dickinson). For adhesion cells, like J774, after phalloidin-FITC labeling, phalloidin incorporated into the cells was extracted by methanol at room temperature for one hour. After spinning down the cell debris, the supernatant was analyzed on Victor plate reader (Perkin Elmer) at $F_{excitation}$ 485nm/$F_{emission}$ 535nm.